Anharmonic phonon flow through molecular-sized junctions

N. Mingo
NASA-Ames Center for Nanotechnology, N229-1 Moffett Field, California 94035, USA
(Received 10 May 2006; revised manuscript received 12 July 2006; published 1 September 2006)

A general many-body nonequilibrium Green's function approach for interacting phonons is developed, and applied to study the thermal conductance of an anharmonic molecular junction between two solid surfaces. We investigate the dependence of the nanojunction's thermal conductance on temperature, force constants, and bond anharmonicity, and identify different parameter regimes. The calculation results display quantum mechanical effects that differ significantly from classical predictions. The anharmonic technique presented extends the scope of fully quantum mechanical Green's function calculations of phonon transport, which until now had been largely restricted to harmonic (or noninteracting phonon) systems. Thus it may provide a powerful tool for the study of lattice thermal conduction in nanoscale systems, such as point contacts, molecular contacts, and interfaces.

DOI: 10.1103/PhysRevB.74.125402 PACS number(s): 63.22.+m, 63.20.Kr, 65.80.+n, 66.70.+f

I. INTRODUCTION

The theory of phonon transport in materials has developed for many decades, its origins dating back to the works of Debye and Peierls.[1,2] For most of this period the focus was on describing macroscopic thermal transport properties of solids, mainly because local nanoscale transport measurements were out of the question. The situation has recently changed, however, for new techniques have been developed that enable the measurement of thermal conduction through nanoscale structures.[3–5] Therefore, an important focus is now being placed on theoretical techniques that address the problem of phonon transport across structures defined at the nanoscale and atomic level.

One line of research in this direction is based on classical molecular dynamics, where effective techniques have been developed to study heat transport across atomically defined interfaces and structures.[6–9] Although these classical techniques lead to important insights on the heat transport process, however they are strictly valid only in the higher temperature regimes, and they do not capture the quantum mechanical aspects of the phonon transport problem. From the point of view of condensed matter physics, it is very important to be able to describe the phonon transport process in fully quantum mechanical terms. This is so, both for fundamental, as well as applied reasons, because there are important features of the transport process that only a quantum mechanical description can capture.

Important advances towards a fully quantum mechanical theory of nanoscale phonon transport have recently been made, many of them via Green's function (GF) methods. Continuum medium GF techniques were used in Refs. 10–13 to describe the quantum transport through nanowires in the presence of surface roughness and at nanowire-bulk contacts. Atomistic GF methods were developed to describe transport through atomic chains,[14] alkane molecules,[15] disordered solid-solid interfaces,[16] and Si nanowires.[17] An alternative formulation with the same philosophy, and leading to the same results, is the method of interface matching lattice dynamics.[18–20] Other important works have addressed different types of nanoscale systems in different conditions.[21–25]

A few studies have modeled anharmonic phonon transport in a fully quantum mechanical way,[22,25,26] although none of these was formulated in terms of Green's functions. A main drawback of the Green's functions methods cited in the preceding paragraph is that they *have not included anharmonicity*. That is a serious limitation, because anharmonicity is an ubiquitous source of phonon scattering in any solid, and it is very important to be able to quantify its effect. In this paper we present a general atomistic nonequilibrium Green's function theory that incorporates the effect of the system's anharmonicity. We also illustrate the application of this technique to describe the phonon transport between two solid surfaces joined by an anharmonic diatomic molecule.

The theory presented here includes anharmonic interactions via a Keldysh diagrammatic approach. The Keldysh formalism[27–30] is a very powerful technique of theoretical physics that has been extensively applied to nonequilibrium electron problems, including inelastic electron tunneling,[31–33] Coulomb blockade,[34,35] photocurrent generation in nanodevices[36,37] and in molecular junctions,[38] and many others. However, up to our knowledge, its application to the flow of interacting phonons has not been investigated before.

The first part of this paper develops the general theory of interacting phonon transport, explicitly deriving all expressions that are particular to the phonon transport case. The theory is expressed in the most general form, and it can be applied to any atomically described solid system. In the second part we present a thorough study of the phonon transport process across a simple but realistic model of an anharmonic molecular junction between two surfaces. Results for the thermal conductance and the effect of anharmonicity are shown for two particular choices of common interatomic potentials: the Lennard-Jones, and the Stillinger-Weber potentials. By mapping the thermal conductance as a function of bond strengths in the molecular system, we identify three different transport regimes. We relate those regimes to the vibrational spectrum of the system. We also identify several purely quantum mechanical effects taking place in the anharmonic scattering process, which are very different from classical predictions. All the results are summarized in Sec. IV.

The general technique presented should be very useful in the study of thermal transport across disordered interfaces,

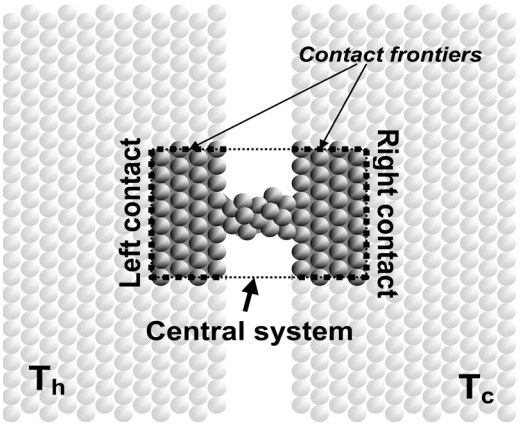

FIG. 1. Typical system configuration in nonequilibrium Green function problems. Many-body interactions are considered inside the central system. The semi-infinite contacts are projected onto the central system via self-energies. The "contact frontiers" are the places where the central system and the contacts join. These frontiers can be arbitrarily placed, and in general do not correspond to any real interface or physical discontinuity.

point junctions, and molecular junctions, for example. It also opens the way to treat the problem of heat dissipation via the lattice, when computing electronic transport in nanoscale and molecular devices. When combined with real-space Green function techniques for linear scaling, the method may become an efficient computational tool for phonon transport in nanoscale and mesoscale systems.

II. THEORY

This section develops the general theory of phonon transport in anharmonic nanoscale systems. We will explicitly show those derivation steps that are specific to phonons, and we will refer to the literature when using general results of nonequilibrium Green function theory that are valid for all systems. For readers unfamiliar with nonequilibrium Green functions, Refs. 28 and 29 are recommended.

The motivation for using Green functions becomes clear in Sec. II D, when we derive the expression for the expected value of the heat current. In general, the expected value of any one-particle operator (such as the heat current) acting on a many-body system can always be expressed in terms of the Green's functions. That is the main motivation to compute the Green functions. We have chosen to place the derivation of the heat current expression after the section on how to compute the Green functions. Although for motivational reasons, the reverse order might seem more proper, Sec. II D uses several definitions that are introduced in Sec. II C, and thus it makes sense to include this part first.

A. System configuration in nonequilibrium Green function problems

Almost all nonequilibrium Green function problems address the same basic topological configuration: two semi-infinite bodies, or reservoirs, joined at a central system. This structure is shown in Fig. 1. The two reservoirs are kept at different temperatures, and therefore a thermal current flows across the central system. The reservoirs are semi-infinite, and the system is in a steady state.

In all cases many-body interactions are treated only inside the central system. This has always been the case in all the fundamental papers devoted to the many-body Keldysh formalism.[29–31,34] Trying to extend the many-body interactions beyond the central system is an extremely complex problem, and we are unaware of any work in that direction. Nonetheless, a crucial point to be understood is that the frontiers defining the central system are arbitrary to some extent. In other words, one can in principle extend these frontiers well within the semi-infinite contacts, to define a fairly large central system, until results do not vary upon further extension.

We remark that the contact frontiers *do not* correspond to any physical interface. The actual physical interface in the problem is located *inside* the central system. This physical interface is the one that limits the phonon transport between the reservoirs. Thus, the largest discontinuity in the local phonon distribution takes place across this physical interface or junction. In contrast, the local phonon distribution across the contact frontiers varies much more slowly, because the current densities at these frontiers, being inside the contact bodies, are smaller.

Because of this, it is crucial to have an accurate description of the phonons near the physical interface. The effect of lattice features becomes less and less important the further away they are from the physical interface. This is why it is possible to include the further parts of the semi-infinite reservoirs, beyond the contact frontiers, in the form of self-energies that are calculated using projection techniques, like the recursion method[40] or the decimation technique.[41] The idea behind these numerical projection methods is that the local Green's functions computed at a selected atomic subset within a cluster converge to those of the truly semi-infinite system when the cluster is made large enough. Techniques in Refs. 40 and 41 give very efficient recipes for systematically enlarging the cluster size until Green function convergence is reached.

Thus, the fact that the interatomic links at the contact frontiers are harmonic (i.e., the many-body interactions are confined into the central system) does not pose any practical restriction to the use of the Keldysh technique. It is enough to push the contact frontiers far enough inside the reservoirs, until the Green functions near the physical interface are well described.

B. Hamiltonian

The quantum mechanical lattice properties of any atomically described system can be represented by the following Hamiltonian:

$$\hat{H} = \frac{1}{2}\sum_{ij} k_{ij}\hat{\varphi}_i\hat{\varphi}_j + \frac{1}{2}\sum_{i} M_i\hat{\varphi}_i\hat{\varphi}_i + \sum_{ijk} V^{(3)}_{ijk}\hat{\varphi}_i\hat{\varphi}_j\hat{\varphi}_k + \cdots . \tag{1}$$

The terms on the right-hand side are the harmonic, kinetic, and anharmonic terms, respectively. $\hat{\varphi}_i$ is the Heisenberg dis-

placement operator for the ith atomic degree of freedom. Here, $k_{ij} \equiv \partial^2 E/\partial u_i \partial u_j$, $V^{(3)}_{ijk} \equiv \frac{1}{3!}\partial^3 E/\partial u_i \partial u_j \partial u_k$, E is the total energy, and the u's are the atomic coordinates. M_i is the mass of the atom to which the ith degree of freedom belongs.

We can also write the Hamiltonian in the orthogonal representation, in terms of the eigenmodes of the harmonic part, as[42]

$$\hat{H} = \sum_q \hbar\omega_q(\hat{b}_q^+ \hat{b}_q + 1/2) + \sum_{ijk} V^{(3)}_{ijk}\hat{\varphi}_i\hat{\varphi}_j\hat{\varphi}_k + \cdots . \quad (2)$$

Here, $\hat{b}_q^+$ and $\hat{b}_q$ are the phonon creation and destruction operators, and the summation is over all the vibrational eigenstates, q. The field operators are expressed in terms of the phonon creation and destruction operators as

$$\hat{\varphi}_j(t) = \sum_q \sqrt{\hbar/M\omega_q}[\hat{b}_q^+ \phi_q^*(j)e^{i\omega_q t} + \hat{b}_q\phi_q(j)e^{-i\omega_q t}],$$

$$\hat{\varphi}_j(t) = \sum_q i\sqrt{\hbar\omega_q/M}[\hat{b}_q^+ \phi_q^*(j)e^{i\omega_q t} - \hat{b}_q\phi_q(j)e^{-i\omega_q t}], \quad (3)$$

where the eigenfunctions $\phi_q(j)$ satisfy

$$\sum_j k_{ij}\phi_q(j) = M_i\omega_q^2\phi_q(i). \quad (4)$$

Inserting Eq. (3) into Eq. (1) and using Eq. (4) one obtains Eq. (2).

To avoid problems arising from the different masses of individual atoms, it is customary to transform the coordinate representation as $\tilde{\hat{\varphi}}_i = \sqrt{M_i/M}\hat{\varphi}_i$, implying $\tilde{k}_{ij} = k_{ij}M/\sqrt{M_iM_j}$, etc. The resulting equivalent problem does not explicitly show the individual masses, but only an overall mass M, which can be arbitrarily chosen without affecting the results. All of the following discussion will thus be in this transformed basis, without explicit reference to individual masses.

C. Computing the interacting-phonon Green functions

Now we explain how to compute the nonequilibrium phonon Green's functions for the type of system described above. The way to compute currents from these Green's functions is shown later in Sec. II D.

There are four interrelated Green's functions:[29] $D^<$, $D^>$, D^R, and D^A. In the time representation they are defined as[42]

$$iD^<_{lm}(t_1 - t_2) \equiv \frac{1}{\hbar}\langle\hat{\varphi}_m(t_2)\hat{\varphi}_l(t_1)\rangle, \quad (5)$$

$$iD^>_{lm}(t_1 - t_2) \equiv \frac{1}{\hbar}\langle\hat{\varphi}_l(t_1)\hat{\varphi}_m(t_2)\rangle, \quad (6)$$

$$iD^R_{lm}(t_1 - t_2) = \frac{1}{\hbar}\Theta(t_1 - t_2)\langle[\hat{\varphi}_l(t_1), \hat{\varphi}_m(t_2)]\rangle, \quad (7)$$

$$iD^A_{lm}(t_1 - t_2) = -\frac{1}{\hbar}\Theta(t_2 - t_1)\langle[\hat{\varphi}_l(t_1), \hat{\varphi}_m(t_2)]\rangle. \quad (8)$$

In steady state problems like the one we want to solve, one does not compute these Green's functions, but their time Fourier transforms. In the noninteracting equilibrium case, such frequency dependent GF's can be expressed in terms of the resolvent, which is a frequency dependent matrix that can be readily computed from the force constants matrix. For the nonequilibrium case, however, one must use "kinetic equations," which involve both the equilibrium and nonequilibrium GF's. The next two sections detail how to obtain the equilibrium and nonequilibrium GF's for phonons, and how to use them in practical computations.

1. Calculation of the uncoupled Green functions at the contacts

Let us consider a case where the central system is decoupled from the contacts, so that all the force constants linking the central system to the contacts are equal to zero. Then no current flows, and the systems are in equilibrium. We will denote these uncoupled Green functions at the contacts by $D_0^<$, D_0^R. The other two GF's are related to these by[28] $D^>_{0,lj}(\omega) = D^<_{0,jl}(-\omega)$, $D^A_{0,lj}(\omega) = [D^R_{0,jl}(\omega)]^*$. The reason why we need to compute these uncoupled GF's is that they enter the expression for the contact self-energies, Eqs. (25) and (26), as we will see in the next section.

We can derive the expression for the unperturbed $D_0^<$ at the contacts in the following way. First we obtain the time-dependent Green's function. For this, we start from its definition, Eq. (5). Using the eigenstate expansions of the field operators, Eq. (3), one obtains

$$iD^<_{0\,lm}(t) = \sum_k \frac{1}{M\omega_k}[(N_{-k}+1)e^{i\omega_k t} + N_k e^{-i\omega_k t}]\phi_k(l)\phi_k^*(m), \quad (9)$$

where N_k is the occupation of eigenstate k, and the summation is over all the eigenstates. Label k is a shorthand notation for a set of quantum numbers, such as the wave vector and the polarization. Label $-k$ denotes the same quantum numbers as k except those for the wave vector, which has the opposite direction.

We are, however, interested in the frequency dependent form of $D_0^<$, which we obtain by Fourier transforming the previous expression,

$$iD^<_{0\,lm}(\omega) = \sum_k \frac{\pi}{M\omega_k}[(1+N_{-k})\delta(\omega+\omega_k) + N_k\delta(\omega-\omega_k)]\phi_k(l)\phi_k^*(m). \quad (10)$$

However this expression, in terms of the eigenfunctions, is not practical for computational purposes. It is much more convenient to express the Green function in terms of the resolvent, $G(\omega^2) \equiv [(\omega+i\delta)^2\mathbf{I} - \mathbf{K}]^{-1}$, where $\mathbf{K}$ is the force constants matrix of the system, defined as $k_{ij} \equiv \frac{1}{\sqrt{M_iM_j}}\frac{\partial^2 E}{\partial u_i \partial u_j}$, and $\delta \to 0$. For this, we use the identity $\delta(x-y) = 2x\delta(x^2-y^2)\Theta(x)$, with $y>0$, and rewrite (10) as

$$iD^<_{0\,lm}(\omega) = \sum_k \frac{\phi_k(l)\phi_k^*(m)}{M} 2\pi\delta(\omega^2 - \omega_k^2) \times[(1+N_{-k})\Theta(-\omega) + N_k\Theta(\omega)]. \quad (11)$$

Now, we use the definition of the spectral density,

$$\rho_{lm}(\omega^2) \equiv \sum_k \phi_k(l)\phi_k^*(m)\delta(\omega^2-\omega_k^2), \tag{12}$$

which substituted in (11) yields, for the equilibrium case

$$D_{0\,ij}^{<} = -\frac{2\pi i}{M}[\Theta(-\omega)\rho_{ij}(\omega^2)+N(\omega^2)\rho_{ij}(\omega^2)], \tag{13}$$

where $N(\omega^2)$ is the equilibrium phonon occupation at frequency ω. This expression is much more convenient for computational purposes, and it only requires to compute ρ.

Now, the spectral density of states, ρ, is directly related to the resolvent, $\mathbf{G}$: we first note that

$$G_{lm}(\omega^2) \equiv \sum_k \frac{\phi_k(l)\phi_k^*(m)}{(\omega+i\delta)^2-\omega_k^2} \tag{14}$$

$$=\sum_k \frac{1}{2\omega_k}\left(\frac{1}{\omega-\omega_k+i\delta}-\frac{1}{\omega+\omega_k+i\delta}\right)\phi_k(l)\phi_k^*(m), \tag{15}$$

which is trivially verified by substitution. The summation in k extends over all the eigenstates of the system. Taking the imaginary of (15), one obtains the spectral density of states, ρ:

$$\begin{aligned}\mathrm{Im}[G_{lm}(\omega^2)] &= \sum_k \frac{\pi\phi_k(l)\phi_k^*(m)}{2\omega_k}[\delta(\omega-\omega_k)-\delta(\omega+\omega_k)] \\ &= \sum_k \pi\phi_k(l)\phi_k^*(m)\delta(\omega^2-\omega_k^2) \equiv \pi\rho_{lm}(\omega^2),\end{aligned} \tag{16}$$

where $\delta\to 0^+$ and $\omega>0$.

Thus, to evaluate $D_0^<$, one only needs to compute the resolvent $\mathbf{G}$, and the Bose occupation factors, N. These occupation factors are different for each of the contacts, because the latter are at two different temperatures.

To obtain the unperturbed retarded Green function we operate similarly. First, the time-dependent form of the retarded Green function, D^R, is obtained directly from its definition, Eq. (7),

$$\begin{aligned} iD_{0\,lm}^R(t) &= \frac{1}{\hbar}\Theta(t)\langle[\hat{\varphi}_l(t),\hat{\varphi}_m(0)]\rangle \\ &= \Theta(t)\left(\sum_q \frac{\phi_q(l)\phi_q^*(m)}{2M\omega_q}[N_q e^{i\omega_q t} \right. \\ &\quad \left. + (1+N_{-q})e^{-i\omega_q t} - N_{-q}e^{-i\omega_q t} - (1+N_q)e^{i\omega_q t}]\right) \\ &= \Theta(t)\sum_q \frac{\phi_q(l)\phi_q^*(m)}{2M\omega_q}(e^{-i\omega_q t}-e^{i\omega_q t}). \end{aligned} \tag{17}$$

For the frequency dependent form, we Fourier transform the previous expression, as

$$D_{0\,lm}^R(\omega) = \sum_q \frac{\phi_q(l)\phi_q^*(m)}{2M\omega_q}\left(\frac{1}{\omega-\omega_q+i\delta}-\frac{1}{\omega+\omega_q+i\delta}\right) \tag{18}$$

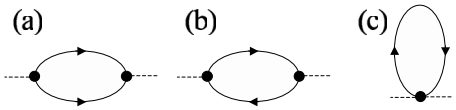

FIG. 2. Lowest order diagrams for three-phonon (a), (b), and four-phonon (c) many-body interactions.

$$=\sum_q \frac{\phi_q(l)\phi_q^*(m)}{2M}\frac{2}{(\omega+i\delta)^2-\omega_q^2}, \tag{19}$$

so finally

$$D_{0\,lm}^R(\omega) = \frac{1}{M}G_{lm}(\omega^2). \tag{20}$$

2. The coupled Green functions

If we couple the system, a net phonon current flows from the hotter to the colder contact, and we no longer have an equilibrium system. The GF's for the coupled system satisfy the Dyson equation,[28] and from it, kinetic equations are derived for the particular GF's. This is a result of the general theory of nonequilibrium GF's. A common way of writing these equations is[29]

$$\mathbf{D}^{<(>)} = \mathbf{D}^R\boldsymbol{\Sigma}^{<(>)}\mathbf{D}^A, \tag{21}$$

$$\mathbf{D}^R = (\omega^2\mathbf{I}-\mathbf{K}-\boldsymbol{\Sigma}^R)^{-1}, \tag{22}$$

$$\mathbf{D}^A = (\mathbf{D}^R)^+. \tag{23}$$

The $\boldsymbol{\Sigma}$'s are self-energy matrices,[28] which consist of a contribution due to the contact leads, $\boldsymbol{\Sigma}_{h(c)}$, plus a many-body contribution from the anharmonic interactions within the island, $\boldsymbol{\Sigma}_M$,

$$\boldsymbol{\Sigma} = \boldsymbol{\Sigma}_M + \boldsymbol{\Sigma}_h + \boldsymbol{\Sigma}_c. \tag{24}$$

It is easily shown[29] that the contributions of the contacts are

$$\boldsymbol{\Sigma}_{h(c)}^{<} = \mathbf{K}_{h(c)}\mathbf{D}_{0\,h(c)}^{<}\mathbf{K}_{h(c)}^T, \tag{25}$$

$$\boldsymbol{\Sigma}_{h(c)}^{R} = \mathbf{K}_{h(c)}\mathbf{D}_{0\,h(c)}^{R}\mathbf{K}_{h(c)}^T, \tag{26}$$

where $\mathbf{K}_{h(c)}$ is the part of the force constants matrix joining the central system to the hot (cold) contact.

3. The many-body self-energies

The many-body contributions to the self-energy are computed from the corresponding Feynman diagrams, following the general rules in Ref. 28. The three-phonon processes are represented by the diagrams in Figs. 2(a) and 2(b), corresponding to the following self-energies:

$$\begin{aligned}\text{(a)}\quad i\Sigma_{M(3)i,n}^{<}(\omega) &= \hbar\sum_{jklm}\int_{-\infty}^{\infty} V_{ijk}^{(3)}D_{jl}^{<}(\omega')D_{km}^{<}(\omega \\ &\quad -\omega')V_{lmn}^{(3)}d\omega', \end{aligned} \tag{27}$$

$$\text{(b)}\quad i\Sigma^{<}_{M(3)i,n}(\omega) = \hbar \sum_{jklm} \int_{-\infty}^{\infty} V^{(3)}_{ijk} D^{>}_{jl}(\omega') D^{<}_{km}(\omega + \omega') V^{(3)}_{lmn} d\omega'. \tag{28}$$

Since[28] $D^{>}_{lj}(\omega) = D^{<}_{jl}(-\omega)$, the two above self-energies are equivalent. This three-phonon self-energy is purely imaginary. Once $\mathbf{\Sigma}^{<(>)}_{M(3)}$ are computed, the $\Sigma^{R(A)}_{M(3)}$ can be obtained from them. Its imaginary part is given by[28]

$$2\ \mathrm{Im}\ \mathbf{\Sigma}^{R}_{M(3)} = \mathbf{\Sigma}^{<}_{M(3)} - \mathbf{\Sigma}^{>}_{M(3)}. \tag{29}$$

The real part is related to the imaginary part by the Hilbert transform[32]

$$\mathrm{Re}\ \mathbf{\Sigma}^{R}_{M(3)} = \mathcal{H}(\mathrm{Im}\ \mathbf{\Sigma}^{R}_{M(3)}). \tag{30}$$

This Hilbert transform is evaluated numerically, by the standard method of convoluting in the Fourier space.

The lowest order four-phonon diagram is that in Fig. 2(c). This diagram does not contribute to $\mathbf{\Sigma}^{<(>)}_{M}$. However, it affects $\mathbf{\Sigma}^{R(A)}_{M}$,

$$i\Sigma^{R}_{M(4)i,j} = \hbar \sum_{kl} \int_{-\infty}^{\infty} V^{(4)}_{iklj} [D^{<}_{kl}(\omega') + D^{>}_{lk}(\omega')] d\omega'. \tag{31}$$

Unlike the three-phonon contribution, this four-phonon contribution is purely real, and independent of frequency. This means that the fourth order diagrams in Fig. 2(c) just modify the force constants, introducing an elastic scattering of the phonons analogous to the Hartree term for electrons. Although four-phonon processes can be important,[39] they have not been included in this paper in order to keep the analysis simpler.

4. Self-consistent procedure

The many-body self-energies involve the total Green's functions. Therefore, in the presence of many-body interactions the calculation needs to be done self-consistently. The complete calculation procedure is as follows. First, the resolvent at the contacts is computed, using projection techniques like those in Refs. 40 or 41 for example. The unperturbed Green's functions at the contacts are then obtained via Eqs. (13) and (20). The contacts' contribution to the self-energy is computed from these Green's functions, via Eqs. (25) and (26). For the first iteration, the many-body self-energies are taken as zero. Then the self-consistent loop starts, by computing successively $\mathbf{D}^{R(A)}$ [Eqs. (22) and (23)], $\mathbf{D}^{>(<)}$ [Eq. (21)], $\mathbf{\Sigma}^{<(>)}$ [Eqs. (24), (27), and (28)], and $\mathbf{\Sigma}^{R(A)}$ [Eqs. (29) and (30)]. This is repeated until convergence is achieved. Afterwards, we can compute the heat current for the self-consistent system.

D. Expression of the heat current

We now derive the expression for the total heat current. Let us consider the atoms at one of the contact frontiers, which are harmonic (see Sec. II A). For each degree of freedom within this subsystem we can define a "local energy" operator,

$$\hat{H}_i = 1/4 \sum_j (\hat{\varphi}_i k_{ij} \hat{\varphi}_j + \hat{\varphi}_j k_{ji} \hat{\varphi}_i) + \frac{M_i}{2} \hat{\dot{\varphi}}_i^2, \tag{32}$$

such that the total Hamiltonian of the subsystem is expressed as

$$\hat{H} = \sum_i \hat{H}_i. \tag{33}$$

The change in local energy with respect to time is then

$$\frac{dE_i}{dt} \equiv \frac{d\langle \hat{H}_i \rangle}{dt} = \left\langle \frac{1}{4} \sum_j \hat{\dot{\varphi}}_i k_{ij} \hat{\varphi}_j + \hat{\varphi}_j k_{ji} \hat{\dot{\varphi}}_i + \hat{\dot{\varphi}}_i k_{ij} \hat{\varphi}_j + \hat{\varphi}_j k_{ji} \hat{\dot{\varphi}}_i + \frac{M_i}{2} (\hat{\ddot{\varphi}}_i \hat{\dot{\varphi}}_i + \hat{\dot{\varphi}}_i \hat{\ddot{\varphi}}_i) \right\rangle, \tag{34}$$

which, using $M_i \hat{\ddot{\varphi}}_i = -\Sigma_j k_{ij} \hat{\varphi}_j$, becomes

$$\frac{dE_i}{dt} = 1/4 \sum_j (\langle \hat{\dot{\varphi}}_i k_{ij} \hat{\varphi}_j \rangle - \langle \hat{\varphi}_i k_{ij} \hat{\dot{\varphi}}_j \rangle) - (\langle \hat{\dot{\varphi}}_j k_{ji} \hat{\varphi}_i \rangle - \langle \hat{\varphi}_j k_{ji} \hat{\dot{\varphi}}_i \rangle) \equiv \sum_j J_{ij}.$$

So we have obtained the expression for the local current between two different degrees of freedom belonging to two mutually interacting atoms. For a steady state, these local energy currents can be expressed in terms of phonon Green's functions as follows:

$$\begin{aligned} J_{ij} &= \frac{1}{4} \lim_{t \to t'} \frac{d}{dt} \{ k_{ji} [\langle \hat{\varphi}_j(t) \hat{\varphi}_i(t') \rangle - \langle \hat{\varphi}_j(t') \hat{\varphi}_i(t) \rangle] \\ &\quad - k_{ij} [\langle \hat{\varphi}_i(t) \hat{\varphi}_j(t') \rangle - \langle \hat{\varphi}_i(t') \hat{\varphi}_j(t) \rangle] \} \\ &= \frac{i\hbar}{4} \lim_{t \to t'} \frac{d}{dt} \{ k_{ij} [D^{<}_{ji}(t,t') - D^{<}_{ji}(t',t)] - k_{ji} [D^{<}_{ij}(t,t') \\ &\quad - D^{<}_{ij}(t',t)] \} = \frac{1}{2} \int_{-\infty}^{\infty} \hbar\omega [k_{ij} D^{<}_{ji}(\omega) - D^{<}_{ij}(\omega) k_{ji}] d\omega / 2\pi. \end{aligned} \tag{35}$$

Here we have used,[28] $D^{<}_{ij}(t_1,t_2) \equiv \frac{-i}{\hbar} \langle \hat{\varphi}_j(t_2) \hat{\varphi}_i(t_1) \rangle = \int_{-\infty}^{\infty} D^{<}_{ij}(\omega) e^{-i\omega(t_2 - t_1)} d\omega / 2\pi$.

Although Eq. (35) already expresses the current in terms of Green functions, we can still obtain a nicer expression, by following the steps given in Ref. 29. To do this, we first define the matrix of "current density," composed of elements that appear in Eq. (35),

$$\mathbf{J}(\omega) = \hbar\omega (\mathbf{K}\mathbf{D}^{<} - \mathbf{D}^{<}\mathbf{K}). \tag{36}$$

From Eq. (35) it is obvious that the trace of this matrix, integrated in frequency, gives the total current coming in and going out of the system. We now use the following equations, which are straightforwardly obtained from the Dyson equation for the retarded or advanced Green function:

$$\mathbf{K}\mathbf{D}^{R} = \omega^2 \mathbf{D}^{R} - \mathbf{\Sigma}^{R} \mathbf{D}^{R} - \mathbf{I}, \tag{37}$$

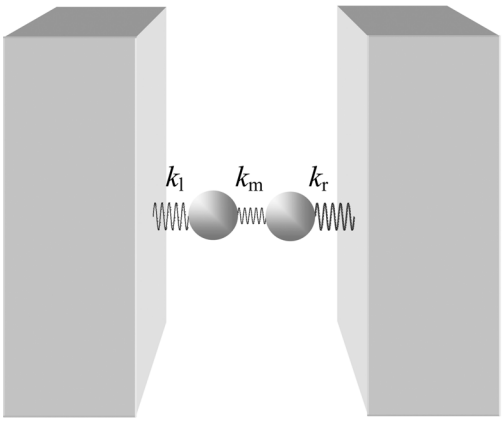

FIG. 3. Configuration of the model molecular junction problem. Two Si atoms are mutually bonded by an anharmonic potential. Each of them is also adsorbed onto a solid surface by a harmonic spring. Only vibrations in the direction perpendicular to the surfaces are considered.

$$\mathbf{D}^A\mathbf{K} = \omega^2\mathbf{D}^A - \mathbf{D}^A\boldsymbol{\Sigma}^A - \mathbf{I}. \tag{38}$$

Substituting expression Eq. (21) into Eq. (36), and using Eqs. (37) and (38), we have

$$\begin{aligned}\mathbf{K}\mathbf{D}^< - \mathbf{D}^<\mathbf{K} &= \mathbf{D}^R\boldsymbol{\Sigma}^<\mathbf{D}^A(\boldsymbol{\Sigma}^A - \boldsymbol{\Sigma}^R) - \boldsymbol{\Sigma}^<\mathbf{D}^A + \mathbf{D}^R\boldsymbol{\Sigma}^< \\ &= \mathbf{D}^<(\boldsymbol{\Sigma}^A - \boldsymbol{\Sigma}^R) - \boldsymbol{\Sigma}^<(\mathbf{D}^A - \mathbf{D}^R) \\ &= \mathbf{D}^<\boldsymbol{\Sigma}^> - \boldsymbol{\Sigma}^<\mathbf{D}^>, \end{aligned} \tag{39}$$

where we have used

$$\boldsymbol{\Sigma}^A - \boldsymbol{\Sigma}^R = \boldsymbol{\Sigma}^> - \boldsymbol{\Sigma}^<, \tag{40}$$

$$\mathbf{D}^A - \mathbf{D}^R = \mathbf{D}^> - \mathbf{D}^<. \tag{41}$$

Therefore, the current frequency distribution at the hot (h) or cold (c) contact interfaces is

$$J_{h(c)}(\omega) = +(-)\mathrm{Tr}(\boldsymbol{\Sigma}^<_{h(c)}\mathbf{D}^> - \boldsymbol{\Sigma}^>_{h(c)}\mathbf{D}^<)\hbar\omega/2\pi. \tag{42}$$

This, integrated in frequency, yields the total heat current. In general, if there are inelastic processes, $J_h(\omega) \neq J_c(\omega)$, but their integrals are the same.

III. APPLICATION: PHONON TRANSPORT THROUGH A MOLECULAR JUNCTION

Let us now apply the general theory developed above to investigate a simple model molecular junction.

A. Description of the molecular junction system

1. System's composition and geometrical configuration

The geometrical configuration of the system is illustrated in Fig. 3. Only motions in the direction perpendicular to the surfaces are considered. Two Si atoms are bonded to each other by an anharmonic potential $V(x)$, and each of them is adsorbed onto one surface, linked by a harmonic spring with constant $k_l = k_r$. The central bond has a spring constant $k_m \equiv \frac{1}{2}\frac{d^2V}{dx^2}|_{x=x_0}$, where x_0 is the equilibrium bond length. Its degree of anharmonicity is related to the potential's third derivative, $V''' \equiv \frac{d^3V}{dx^3}|_{x=x_0}$.

The system we study is perhaps the simplest model that contains all the aspects of any complex phonon flow problem: several degrees of freedom, surfaces with a frequency dependent density of states, and anharmonicity "inside" the bonds. Let us briefly discuss the significance of these three aspects.

(1) *Several degrees of freedom*. The system contains two atoms, and it considers vibrations in the x direction, perpendicular to the surfaces. This is the smallest system for which the Green functions are matrices. If we had considered a one atom system, the Green functions would be scalars, for which the implementation is simpler, but does not contain the complexity involved in the general problem. We chose the diatomic 2×2 matrix problem for the sake of conceptual clarity. We could have considered a larger number of degrees of freedom, but this would not make any qualitative difference in the treatment, and it would unnecessarily complicate the model.

(2) *Frequency dependent surface density of states*. Some model studies of electron transport across molecular systems have simplified the surfaces by assuming a constant density of states. This would be a very unrealistic assumption in the problem studied here, for it is known[21,43] that the phonon spectral density at a surface is proportional to ω, and it has a finite range. Our model surface contains these aspects and it is the simplest model that yields a realistic representation of the vibrational structure of a solid surface.

(3) *Anharmonicity "inside" the bond*. There are simpler systems that contain anharmonicity: for example, one can consider the atoms linked to an *external* anharmonic potential. In that case, anharmonicity enters only as a scalar self-energy $\Sigma^<_\phi$. Although such scalar self-energy is easier to treat, it is neither a system one encounters in nature, nor does it reflect the complexity of typical systems where anharmonicity enters at the bonds between atoms. In general, anharmonicity is a property of the bonds between different atoms, and it introduces a matrix self-energy, which our model correctly accounts for.

We could include anharmonicity in the surface-molecule bonds also. To do this, the "contact frontiers" (see Fig. 1) must be placed further inside the solids, so that the central system contains more than just two atoms. However, this would complicate the model, going against the goal of conceptual clarity pursued here. An additional argument justifies choosing the central bond, rather than the surface-molecule bond, to be the anharmonic one. The reason is that the surface-molecule bond is in fact the sum of multiple bonds between one atom at the molecule and many atoms at the surface. Therefore, this interaction potential is deeper, and its total spring constant larger, than that of a single bond between two atoms. Now, the deeper the potential, the less the anharmonicity is manifested, or conversely, looser bonds allow atoms to stretch further into the anharmonic range than tighter bonds do. Therefore, it is physically more meaningful to have an anharmonic central bond and treat the surface-molecule bonds as harmonic.

The mass of all the atoms was chosen to be that of Si. The phonon frequency range at the contact surfaces was chosen to be 100 THz, roughly the extent of the phonon spectrum in bulk Si. The calculation of surface Green functions and self-energies is described in Sec. III A 3 below.

With the specifications above, our molecular system is determined by three physical parameters: the molecule's internal spring constant, k_m, the molecule's anharmonicity constant, V''', and the spring constants, $k_l=k_r$, between the surfaces and the molecule. Each of these parameters can vary in a very wide range, spanning different orders of magnitude. In Secs. III B–III D below, we map the dependence of the thermal conductance on all these parameters, and the temperature.

2. Interatomic potentials

The atomic interactions within a system can be computed in multiple ways, ranging from total energy first-principles calculations to parametrized interatomic potentials available in the literature. No matter which method one uses, the goal is to obtain the force constant matrix, $d^2E/du_i du_j$, and the anharmonic constant tensor, $d^3E/du_i du_j du_k$.

Two examples of well known potentials describing atomic interactions are the Lennard-Jones (LJ) potential,[44] and the Stillinger-Weber (SW) potential.[45] The former has been widely used to describe atomic and molecular adsorption. The latter is a potential specifically developed to describe bulk Si. In our study, we present general results for any potential in a wide range of force constant and anharmonicity values. Nevertheless, it is worth focusing on the LJ and SW potentials in order to get a feeling of the actual orders of magnitude which are typical in physical systems.

The LJ potential is defined as

$$V(x) = 4\epsilon[(\xi/x)^{12} - (\xi/x)^6], \tag{43}$$

where x is the interatomic distance. The potential contains a multiplicative constant, ϵ, which is chosen to yield an appropriate potential depth, depending on the system considered. For chemisorbed or strongly bound atoms, the potential depth will be in the order of eV, but for physisorbed or weakly bound atoms it can be several orders of magnitude smaller. Constant ξ is chosen to yield a minimum at the proper bond length. In the calculations presented here, we use $\xi=2.0951$ Å, which yields the potential minimum at $x_0=2.35$ Å, the bond length of bulk Si. Therefore, the force and anharmonic constants of our LJ potential are related by

$$\left.\frac{d^3V}{dx^3}\right|_{x=x_0}^{\mathrm{LJ}} = \left.\frac{d^2V}{dx^2}\right|_{x=x_0}^{\mathrm{LJ}} 8.94/\text{Å}. \tag{44}$$

In the next sections we will use this relation to calculate the thermal conductance change induced by anharmonicity, for different ranges in the strength of the bond, $\left.\frac{d^2V}{dx^2}\right|_{x=x_0}$, or equivalently, the potential depth.

The two-body term of the SW potential has the form

$$V(x) = A(Bx^{-4} - 1)e^{1/(x/\xi - a)}, \quad x/\xi < a,$$

$$V(x) = 0, \quad x/\xi > a, \tag{45}$$

where $B=0.602\,224\,558\,4$, and $a=1.80$. (For the example, we will only address the two-body term in the SW potential.)

In the case of the SW potential the relation equivalent to Eq. (44) is

$$\left.\frac{d^3V}{dx^3}\right|_{x=x_0}^{\mathrm{SW}} = \left.\frac{d^2V}{dx^2}\right|_{x=x_0}^{\mathrm{SW}} 2.46/\text{Å}. \tag{46}$$

Thus, the LJ potential is much more anharmonic than the SW potential. Although strictly speaking the SW potential has a fixed depth of −2.17 eV, in the following sections we will vary the potential depth, in analogy to the LJ case, in order to compare between the two potentials. In Sec. III D 3 we will see how, due to its larger anharmonicity, the LJ potential yields much larger deviations of the thermal conductance with respect to the harmonic case than the SW potential.

3. Surface Green's function and self- energy

It is known that the spectral density of states at a solid surface is, in the lower frequency limit, proportional to the frequency.[21,43] In other words, $\rho(\omega)=\frac{1}{2\pi}\,\mathrm{Im}[G(\omega)]\propto\omega$. We give a proof of this in the Appendix. In addition, from general properties of Green's functions, we know that the onsite integral $\int_0^\infty \rho_{ii}(\omega^2)d\omega^2=1$, for any atomic degree of freedom i.[42] Therefore, a qualitatively correct representation of the surface spectral density is

$$\rho = \frac{3}{2}\frac{\omega}{\omega_D^3}\Theta(\omega_D - \omega), \tag{47}$$

where ω_D is the upper frequency limit in the solid, in our case 100 THz, and Θ is the step function.

To compute the real part of the resolvent we Hilbert transform its imaginary part. This is the *bare* surface retarded Green's function. Now we need to alter it to account for the presence of the molecule. This is because, whenever a nondiagonal element k_{ij} is added into the force constants matrix of the system, two corresponding diagonal elements $k_{ii}=k_{jj}=-k_{ij}$ must be added as well, to satisfy momentum conservation. In our case, we want to compute the self-energy

$$\Sigma_{l(r)}^R(\omega) = k_{l(r)}^2 G_{l(r)}(\omega^2), \tag{48}$$

which contains the effect of the left (right) contact surface onto the molecule. To obtain G in the presence of the molecule, we use the Dyson equation, $G=G_{\mathrm{bare}}-G_{\mathrm{bare}}k_l G$, accounting for the modification of the diagonal force constant at the surface by an amount $-k_l$. This implies

$$G_{l(r)} = G_{\mathrm{bare}}[1 + k_{l(r)}G_{\mathrm{bare}}]^{-1}. \tag{49}$$

More realistic calculations of surface self-energies can be carried out using the decimation technique,[41] or the recursion method,[40] for example. This however requires a prior knowledge of the surface atomic structure. In many cases, real surfaces display reconstructions. In addition, surface states specific to the particular system may exist. Such features

would blur the fundamental physical picture conveyed in this paper, and therefore they will not be considered here.

4. Computational implementation

For each particular set of values k_m, $k_l=k_r$, V''', and T_c, the phonon current was self-consistently computed. In all cases the temperature of the hotter side was 1.5 times that of the colder side, $T_h=1.5T_c$. Since the substrate vibrational frequencies range between 0 and 100 THz, all conduction takes place in this frequency interval. However, the Green's functions are nonzero outside this range as well. It is mandatory to consider this extended frequency range, because we are using Hilbert transforms in the calculation [Eq. (30)], which would not be accurate otherwise. We verified that a frequency range of 300 THz is enough to yield accurate results. The frequency range was divided in steps of 0.5 THz, and the Green's functions were calculated at each of those frequencies, both for ω and $-\omega$. The calculation's bottleneck is the double integral in the three-phonon self-energy, Eq. (27). For this integral, frequency steps of 2.5 THz were used, and results were interpolated at frequencies between the steps. We verified that results do not change if these steps are made smaller, within the physical parameter ranges considered in this paper. If however one wants to consider values of $k_l < 0.2\text{eV}/\text{Å}^2$, such step sizes are comparable to the width of the peaks in the vibrational density of states, and therefore the step sizes need to be reduced.

Self-consistency was implemented via an iterative mixing algorithm. After each iteration n, the computed many-body self-energy, $\Sigma_\phi^{<(n)}$ is mixed with the previous one, $\Sigma_\phi^{<\text{mix}(n)} = f\Sigma_\phi^{<(n)} + (1-f)\Sigma_\phi^{<(n-1)}$, with $0<f<1$. The mixed self-energy is then used as an input for the next iteration. The value of f is initially set as 0.5, and the convergence is monitored at every step by computing the quantity

$$s^{(n)} = \sum_{ij} (a_{ij} - b_{ij})^2 \Big/ \sum_{ij} (a_{ij}^2 + b_{ij}^2), \tag{50}$$

where $a_{ij} \equiv \Sigma_\phi^{<(n)}$ and $b_{ij} \equiv \Sigma_\phi^{<\text{mix}(n-1)}$. Self-consistency is achieved when the input and output self-energies are equal. The results in this paper were converged with a tolerance $s < 10^{-5}$. Using a smaller tolerance did not produce any significant difference.

The value of f was varied dynamically to accelerate convergence. If s increased from one step to the next, f was reduced to 1/5 of its previous value. If s decreased, f was enlarged to 2 times its previous value, up to a maximum of 0.5. If s increased for three consecutive steps, then f was reset to 0.5 again. This empirical procedure allowed us to obtain convergence in less than 15–20 iterations in most cases. This is just one way of obtaining a faster convergence. There are many other algorithms in the literature that can be used to further accelerate the convergence.[46]

In cases when the temperature, or the anharmonicity, were too large, the self-consistent procedure did not converge. There is a physical reason for this. Since we are only including up to third derivatives of the potential, the force between two atoms keeps them bonded only if their separation does not exceed a certain limit. If the energy barrier for this is comparable to or less than k_BT, for too large temperature or too large anharmonicity, then the system becomes unstable. For example, the curve in Fig. 4 corresponding to the LJ potential case did not converge for $T>600$ K.

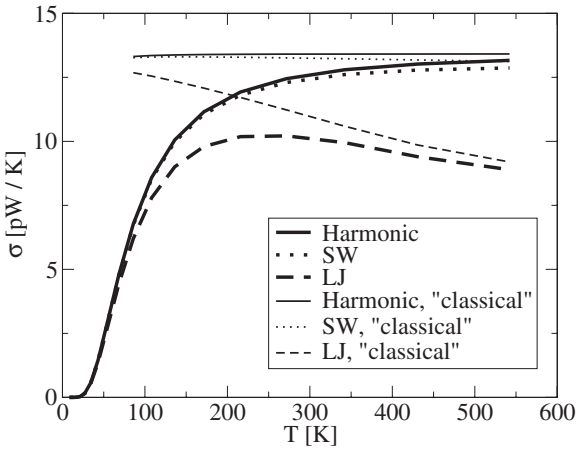

FIG. 4. Temperature dependence of the thermal conductance across the molecular junction, for different degrees of bond anharmonicity. Thick lines show the fully quantum mechanical results. Thin lines show the classical limit, obtained by making $\hbar$ artificially small (see text). The solid lines correspond to a fully harmonic intramoleular bond. Dotted and dashed lines correspond to intramolecular potentials of the Stillinger-Weber and Lennard-Jones type, respectively. The spring constants are $k_m=0.316\ \text{eV}/\text{Å}^2$ and $k_l=3.16\ \text{eV}/\text{Å}^2$.

B. General temperature dependence

Typical curves of thermal conductance versus T are shown in Fig. 4. In general, the conductance increases with temperature, and tends to a saturation at high temperatures. For anharmonic molecules, the conductivity deviates from the harmonic results, this deviation being larger at higher T (see Sec. III D).

For comparison, curves corresponding to the "classical" limit are also shown in Fig. 4. These curves were obtained by doing the calculation using a value of $\hbar$ 10 times smaller than the real one. As expected, the classical results do not show the reduction at low temperatures present in the quantum mechanical case. This phenomenon is analogous to the well known comparison between the quantum mechanical and classical (Dulong and Petit) results for the specific heat.[47] At high temperature the classical and quantum mechanical results converge.

The low temperature thermal conductance of a molecular junction depends as T^3. This is a consequence of the linear frequency dependence of the spectral density of states at the surfaces, and it was already pointed out in Ref. 21. We refer to that work for further details. In what follows, we analyze other aspects of the thermal conductance which have not been investigated before.

C. Three harmonic regimes

Our first task is to understand how the thermal conductance of harmonic junctions depends on the spring constants

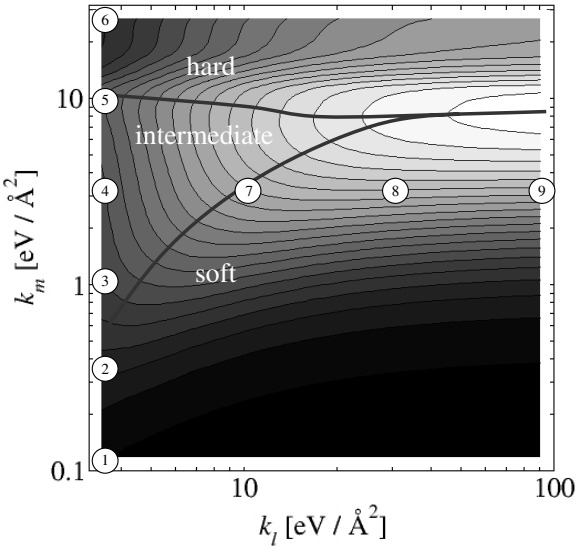

FIG. 5. Plot of the saturated harmonic thermal conductance (at 1000 K), as a function of the intramolecular (k_m) and molecule-surface (k_l) spring constants. The thick lines divide the three harmonic regimes, from top to bottom: hard-molecule, intermediate, and soft molecule. Circled numbers label the parameter locations corresponding to the transmission functions of Fig. 6.

k_l and k_m. k_l can range from a weakly physisorbed interaction to a strongly chemisorbed system. k_m can vary between the almost dissociated bond and the hard molecule case. Therefore, we have mapped the high temperature saturation limit of the thermal conductance, as a function of k_m and k_l in Fig. 5.

Three distinct regions are observable in the map's topography. They can be described as a "hard," "intermediate," and "soft" molecule regimes. The hard molecule regime is intuitively understood: when k_m is very strong the molecule acts as a single rigid object, its internal motion having a much higher frequency than the heat transporting modes. Therefore, in this regime the saturated conductance does not depend on k_m.

The three regimes are well explained in terms of the harmonic transmission function, $\mathcal{T}(\omega)$. The transmission function is readily computed from the retarded Green functions of the system, and it relates to the harmonic thermal conductance by[17]

$$\sigma_{\text{harmonic}} = \frac{1}{2\pi}\int_0^\infty \hbar\omega\mathcal{T}(\omega)\frac{\partial N}{\partial T}d\omega. \tag{51}$$

Peaks in the transmission function give us information about the modes and frequencies that carry the heat. We plot $\mathcal{T}(\omega)$ at different points of the harmonic map of Fig. 5 in Fig. 6. Then we see how peaks, corresponding to the molecule's translational and internal degrees of freedom, shift as a function of the position in the harmonic map.

By increasing k_m, the molecule's internal stretch frequency increases. When it gets out of the solid substrate's allowed frequency range (100 THz), we enter the hard molecule regime. When we increase k_l, on the other hand, the

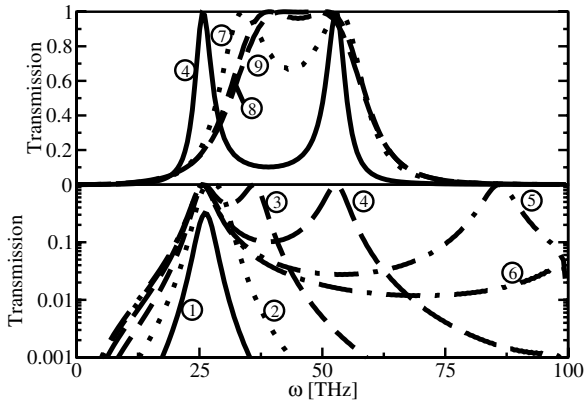

FIG. 6. Harmonic transmission functions corresponding to molecules in different harmonic regimes. Each of the curves is associated to a circled number, corresponding to two particular values of the spring constants k_m and k_l, which can be found in Fig. 5. When a molecule belongs to the intermediate regime, its transmission function shows two clear peaks. In the soft regime the peaks merge into one, and in the hard regime the peak associated with the internal stretch gets out of the range of frequency.

molecule's translational frequency increases. In the intermediate regime, two clear peaks exist, which means that the molecule's internal bond is comparable to the adsorption bonds between the molecule and the surfaces. If the adsorption bonds become much stronger than the internal bond, however, then only one broad peak appears, and the system is in the soft molecule regime.

The harmonic map's topography along several cut lines is shown in Fig. 7. From the cuts we can see the different plateaus taking place in the different harmonic regimes.

D. Anharmonic behavior

1. Temperature dependence of anharmonic effects

Figure 4 shows that at high enough temperature the effect of anharmonicity can be appreciable. To quantify this effect,

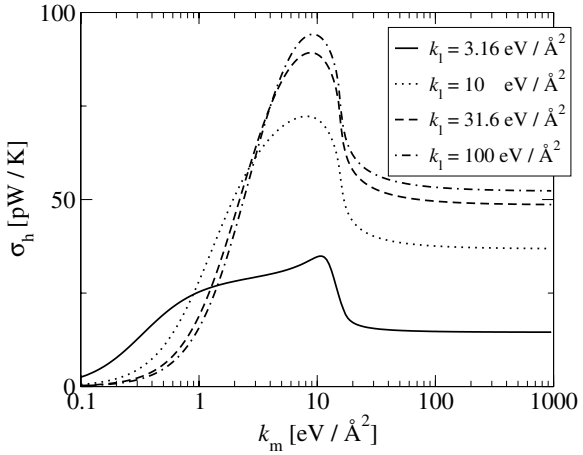

FIG. 7. Plots of harmonic thermal conductance in the saturated limit (at 1000 K), as a function of the intramolecular spring constant, for four different values of the molecule-surface spring constant, k_l. Each of the curves corresponds to a cut along a vertical line in the graph of Fig. 5.

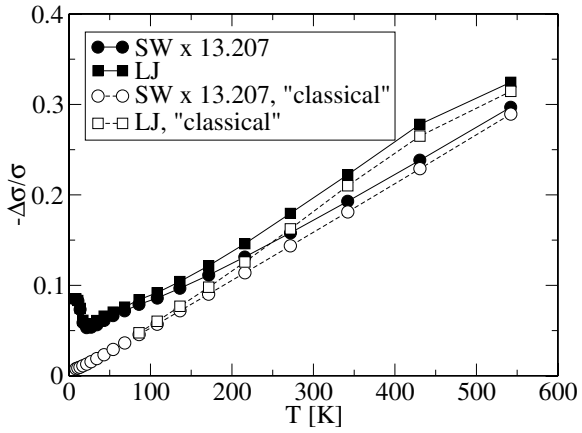

FIG. 8. Relative decrease in thermal conductance due to anharmonicity, as a function of temperature. The case shown corresponds to $k_l=3.16$, $k_m=0.316$. The curves corresponding to the Stillinger-Weber-type potential have been multiplied by $(\beta_{\mathrm{LJ}}/\beta_{\mathrm{SW}})^2=13.207$, for easier comparison with the curves corresponding to the Lennard-Jones potential. See explanations in text.

in Fig. 8 we plot the difference between the harmonic and anharmonic thermal conductance, $\Delta\sigma=\sigma_a-\sigma_h$, normalized by the harmonic conductance, as a function of temperature, for different values of the anharmonic constant, $V''' \equiv \frac{d^3V}{dx^3}|_{x=x_0}$. We see that anharmonic deviations become more important as T increases, behaving approximately as $\Delta\sigma/\sigma_h \propto T$, except at low temperature. We also note that the deviation increases with the square of the anharmonicity, in the form

$$\Delta\sigma/\sigma_h = T\frac{B}{2}\beta^2 + \mathcal{O}(\beta^4), \tag{52}$$

where, β is defined for the particular interatomic potential $V(x)=\frac{1}{2!}V''(x-x_0)^2+\frac{1}{3!}V'''(x-x_0)^3+\ldots$, as

$$\beta \equiv V'''/V''. \tag{53}$$

(x and x_0 are the instantaneous and equilibrium interatomic distances, respectively.) B is a factor independent of β, but dependent on T, and $\mathcal{O}(\beta^4)$ is a small contribution from terms of order β^4 and higher.

2. Quantum mechanical effects

We already saw in Fig. 4 that one particular quantum effect is that the thermal conductivity vanishes at zero temperature. Now, we find another strictly quantum mechanical effect related to the effect of anharmonicity at low temperatures. Looking again at Fig. 8, we see that the relative change in thermal conductance does not vanish when the temperature tends to zero, but instead remains finite. In contrast, in the classical case (numerically mimicked by using an artificial $\hbar$ 10 times smaller than the real one), the effect of anharmonicity, $\Delta\sigma/\sigma$ is still proportional to T at low temperature.

What this means is that *anharmonicity still affects transport even in the zero temperature limit*. This is a consequence of the uncertainty principle: even at $T=0$ lattice vibrations have a certain small but finite amplitude. Therefore, any higher order modification of the quadratic potentials in which they oscillate will have an effect in their zero point frequency. This does not happen classically, because then the spatial extension of the wave functions becomes zero.

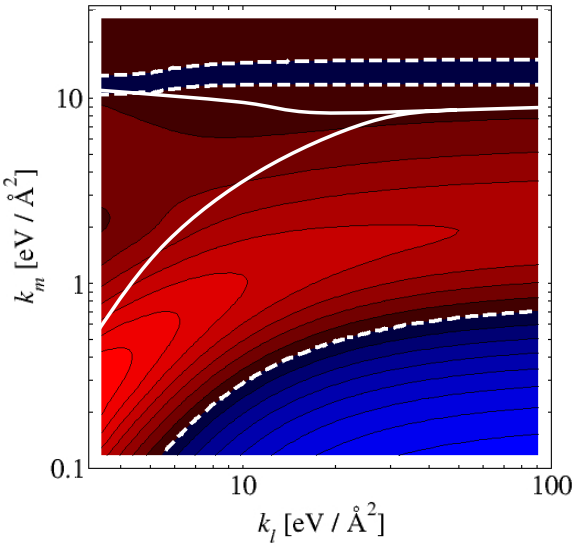

FIG. 9. (Color online) Relative change in thermal conductance due to the presence of anharmonicity, at $T=300$ K, as a function of the spring constants k_m and k_l. Red tones indicate that there is a relative decrease in thermal conductance, whereas blue tones indicate relative increase. Dashed lines correspond to zero level curves, dividing between increase and decrease areas. The thick solid lines separate the three harmonic regimes identified in Fig. 5.

The fact that the calculation captures this subtle quantum mechanical effect reassures us that this method yields the correct description of the many-body phonon flow process.

3. Map of anharmonic effects

The term in β^2 in Eq. (52) is a very useful magnitude, because it provides an estimate of the size of the anharmonic effects for any real interatomic potential. More concretely, we will plot

$$B = \frac{1}{T}\frac{d\Delta\sigma/\sigma_h}{d(\beta^2)}. \tag{54}$$

For the Lennard-Jones potential, $\beta \simeq 8.94$ Å^{-1}, and for the two-body term of the Stillinger-Weber potential it is $\beta \simeq 2.46$ Å^{-1}.

We plot $B(k_l,k_m)$ at $T=300$ K, in Fig. 9. Because of the approximately linear temperature dependence of B, the 300 K plot allows to estimate the effect of anharmonicity at other temperatures as well. Black lines in the map divide the three harmonic regimes obtained in the preceding section.

We see that in the hard molecule regime, internal anharmonic effects are almost negligible. This is to be expected, as the internal degree of freedom almost does not contribute to transport. The border of the hard molecule regime runs parallel and very close to a $B=0$ level curve in the anharmonic map. In contrast, the anharmonic map shows no sharp dis-

continuity between the intermediate and soft molecule region. Two salient features are the following:

(1) the presence of a maximum in the $|B(k_m)|$ curve, for fixed k_l, and

(2) the existence of a $B>0$ region, where the effect of anharmonicity is to increase the total conductance, rather than decrease it.

The $B>0$ values appear when the molecule's internal bond is very weak (i.e., k_m is small). To understand this, let us first think of a harmonic molecule. In such weak bond limit, interaction between the hot and cold sides of the junction is extremely weak, and the thermal conductance tends to zero. If we now allow some small degree of anharmonicity, the interaction between the hot and cold sides is enhanced, and the thermal conductance necessarily increases (it cannot decrease because it is a positive magnitude.)

A narrow region of $B>0$ exists also just above the "hard" regime's border. It's origin in this case is related to the fact that the internal stretch frequency is above, but very close to, the substrate's upper frequency limit. In the presence of anharmonicity, this internal stretch can still contribute to the current slightly, via inelastic effects, and thus slightly enhance the thermal conductance.

The presence of the $|B(k_m)|$ maximum is then understandable. Anharmonic effects must get smaller with increasing k_m, for large enough k_m, because vibrations get confined to the harmonic part of the potential. If k_m is very small, on the other hand, B changes sign, as we explained earlier. Therefore, $|B(k_m)|$ should peak between these two limits. The position of this peak shifts towards smaller k_m, and its magnitude increases, when k_l is reduced. Intuitively, this means that anharmonic effects are more marked when bonds are weak enough and allow for large interatomic bond distortions.

Cuts of the anharmonic map along several lines are shown in Fig. 10. To put these results in concrete terms, the scale on the right-hand side estimates the percentage change in thermal conductance with respect to the harmonic value, at 300 K, for the Lennard-Jones (numbers in brackets), and the Stillinger-Weber potentials. The thermal conductance change due to anharmonicity is about one order of magnitude larger for the LJ than for the SW potential, due to its quadratic dependence on β.

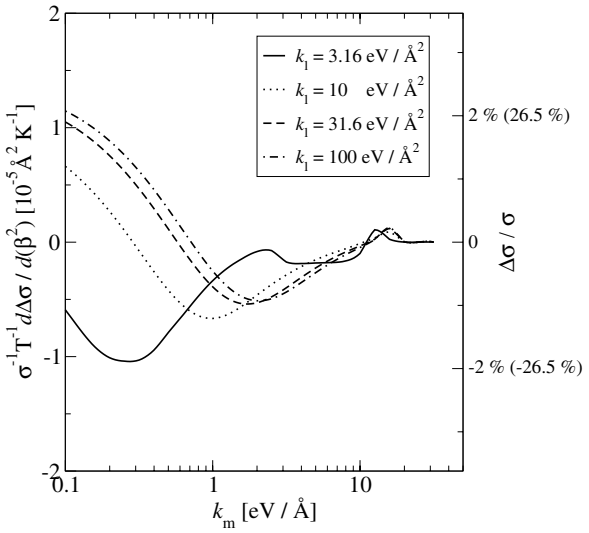

FIG. 10. Plots of the first order change in thermal conductance induced by anharmonicity, as a function of k_m, for different values of k_l. The scale on the right indicates how these values translate in percent change for the Stillinger-Weber potential (no brackets), and for the Lennard-Jones potential (numbers in brackets).

IV. CONCLUSIONS

We have presented a general nonequilibrium Green's function theory of phonon transport through atomically described anharmonic systems. Using this technique, we have performed a thorough study of the thermal transport between two solid surfaces joined by a diatomic molecule.

The general behavior of the thermal conductance as a function of temperature, internal bond strength, and molecule-surface force constant, was shown. Three qualitatively different parameter ranges were identified in relation to the harmonic thermal conductance, and related to general features of the vibrational spectrum. We found that anharmonicity in the molecule changes the thermal conductance by an amount that at high temperatures is roughly proportional to the temperature. At low temperature, a purely quantum mechanical effect takes place, by which anharmonicity still affects the thermal conductivity all the way down to 0 K. It was also found that the effect of anharmonicity is much stronger in a molecule whose internal bond is of the Lennard-Jones type than in one of the Stillinger-Weber type. Detailed maps of harmonic and anharmonic effects as a function of the molecular and adsorption parameters were presented.

The technique developed and demonstrated here brings in anharmonicity into Green function calculations of phonon transport. Therefore, we now have a fully quantum mechanical approach to lattice thermal transport that includes virtually all possible phonon scattering mechanisms existing in a dielectric. Immense possibilities lay ahead in the application of this method to many structures of scientific interest, and in its combined use together with *ab initio* methods, for the quantum-mechanical study of nanoscale thermal transport phenomena.

ACKNOWLEDGMENTS

The author is grateful to D. A. Broido, D. A. Stewart, K. Esfarjani, J. Feldman, and K. Makoshi for helpful discussions.

APPENDIX: PHONON SPECTRAL DENSITY AT A SURFACE

The phonon spectral density at a surface has been shown to depend on frequency as $\propto\omega$, using laborious elastic medium derivations.[21] Nevertheless, one can extract this same conclusion quite simply using Green function reasoning for a discrete lattice system.

First of all, we remember the simple case of a semi-infinite one-dimensional chain. For a 1D chain, the reduced force constant matrix has only nearest neighbor interactions, $k_n=t$, and diagonal elements of magnitude $k_d=-2t$. On the last chain site, which we shall label as "0," the diagonal element is only $k_0=-t$ instead of $-2t$, because this site has only one neighbor.

By quite straightforward application of the Dyson equation, one obtains that the resolvent at the last chain site is

$$G_0 = \frac{E - 2t - \sqrt{E^2 - 4t^2}}{2t(2t - E)}, \tag{A1}$$

where $E \equiv 2t - \omega^2$. The spectral density is given by the imaginary part of this,

$$\mathrm{Im}(G_0) = \frac{\sqrt{4t^2 - E^2}}{2t(2t - E)} = \frac{\sqrt{\omega^4 - 4t\omega^2}}{2t\omega^2}. \tag{A2}$$

When $\omega \to 0$, this gives

$$\mathrm{Im}(G_0) \propto \frac{1}{\omega}. \tag{A3}$$

In the case of a real 3D surface, we can split the problem into multiple independent problems, each one corresponding to a different wave vector parallel to the surface, $\vec{q}_\parallel$. Because of parallel momentum conservation, each of these problems is completely decoupled from the rest, and can be described by an effective one-dimensional system. Now, instead of having $-2t$ for the diagonal elements, we must take into account the dispersion parallel to the surface, so the diagonal elements are $k_d=-2t+c^2q_\parallel^2$ at the inner layers, and $k_0=-t+c^2q_\parallel^2$ at the surface layer. Here c is the sound velocity. So instead of Eq. (A3), we have

$$\mathrm{Im}[G_0(q_\parallel)] \propto 1/\sqrt{\omega^2 - c^2q_\parallel^2}. \tag{A4}$$

The total spectral density is obtained integrating this over $\vec{q}_\parallel$,

$$\rho \propto \int_0^{\omega/c} (\omega^2 - c^2q_\parallel^2)^{1/2} q_\parallel dq_\parallel \propto \omega. \tag{A5}$$

[1] R. Peierls, Ann. Phys. **3**, 1055 (1929).
[2] J. M. Ziman, *Electrons and Phonons* (Oxford University Press, Oxford, 1963).
[3] K. Schwab, E. A. Henriksen, J. M. Worlock, and M. L. Roukes, Nature (London) **404**, 974 (2000).
[4] P. Kim, L. Shi, A. Majumdar, and P. L. McEuen, Phys. Rev. Lett. **87**, 215502 (2001).
[5] D. Li, Y. Wu, P. Kim, L. Shi, P. Yang, and A. Majumdar, Appl. Phys. Lett. **83**, 2934 (2003).
[6] S. T. Huxtable, D. G. Cahill, S. Shenogin, L. Xue, R. Ozisik, P. Barone, M. Usrey, M. S. Strano, G. Siddons, M. Shim, and P. Keblinski, Nat. Mater. **2**, 731 (2003).
[7] P. K. Schelling, S. R. Phillpot, and P. Keblinski, Appl. Phys. Lett. **80**, 2484 (2002).
[8] B. Li, J. Lan, and L. Wang, Phys. Rev. Lett. **95**, 104302 (2005).
[9] O. V. Gendelman and A. V. Savin, Phys. Rev. Lett. **84**, 2381 (2000).
[10] A. Kambili, G. Fagas, V. I. Fal'ko, and C. J. Lambert, Phys. Rev. B **60**, 15593 (1999).
[11] D. H. Santamore and M. C. Cross, Phys. Rev. B **63**, 184306 (2001); D. H. Santamore and M. C. Cross, *ibid.* **66**, 144302 (2002); D. H. Santamore and M. C. Cross, Phys. Rev. Lett. **87**, 115502 (2001); M. C. Cross and R. Lifshitz, Phys. Rev. B **64**, 085324 (2001).
[12] C.-M. Chang and M. R. Geller, Phys. Rev. B **71**, 125304 (2005).
[13] D. E. Angelescu, M. C. Cross, and M. L. Roukes, Superlattices Microstruct. **23**, 673 (1998).
[14] A. Ozpineci and S. Ciraci, Phys. Rev. B **63**, 125415 (2001); A. Buldum, S. Ciraci, and C. Y. Fong, J. Phys.: Condens. Matter **12**, 3349 (2000); S. Ciraci, A. Buldum, and I. P. Batra, *ibid.* **13**, R537 (2001).
[15] D. Segal, A. Nitzan, and P. Hänggi, J. Chem. Phys. **119**, 6840 (2003).
[16] G. Fagas, A. G. Kozorezov, C. J. Lambert, J. K. Wigmore, A. Peacock, A. Poelaert, and R. den Hartog, Phys. Rev. B **60**, 6459 (1999).
[17] N. Mingo and Liu Yang, Phys. Rev. B **68**, 245406 (2003).
[18] D. A. Young and H. J. Maris, Phys. Rev. B **40**, 3685 (1989).
[19] S. Pettersson and G. D. Mahan, Phys. Rev. B **42**, 7386 (1990).
[20] J. Wang and J. S. Wang, Phys. Rev. B **74**, 054303 (2006).
[21] M. P. Blencowe, Phys. Rev. B **59**, 4992 (1999).
[22] D. M. Leitner and P. G. Wolynes, Phys. Rev. E **61**, 2902 (2000).
[23] K. R. Patton and M. R. Geller, Phys. Rev. B **64**, 155320 (2001).
[24] P. B. Allen and J. L. Feldman, Phys. Rev. B **48**, 12581 (1993).
[25] D. Segal and A. Nitzan, Phys. Rev. Lett. **94**, 034301 (2005).
[26] H. Böttger, T. Damker, and V. V. Bryksin, Phys. Status Solidi B **205**, 97 (1998).
[27] L. V. Keldysh, Sov. Phys. JETP **20**, 1018 (1965).
[28] E. M. Lifshitz and L. P. Pitaevskii, *Physical Kinetics*, Course of Theoretical Physics (Pergamon, Oxford, 1981), Vol. 10.
[29] S. Datta, *Electronic Transport in Mesoscopic Systems* (Cambridge University Press, Cambridge, 1995).
[30] A. P. Jauho, N. S. Wingreen, and Y. Meir, Phys. Rev. B **50**, 5528 (1994); H. Haug and A.-P. Jauho, *Quantum Kinetics in Transport and Optics of Semiconductors* (Springer, Berlin, 1996).
[31] R. Combescot, J. Phys. C **4**, 2611 (1971).
[32] E. V. Anda and F. Flores, J. Phys.: Condens. Matter **2**, 8023 (1991).
[33] R. Lake and S. Datta, Phys. Rev. B **45**, 6670 (1992); **46**, 4757 (1992).
[34] Y. Meir and N. S. Wingreen, Phys. Rev. Lett. **68**, 2512 (1992).
[35] K. Makoshi and T. Mii, Surf. Sci. **357-358**, 335 (1995).
[36] L. E. Henrickson, J. Appl. Phys. **91**, 6273 (2002).
[37] D. A. Stewart and F. Leonard, Phys. Rev. Lett. **93**, 107401 (2004).
[38] M. Galperin and A. Nitzan, Phys. Rev. Lett. **95**, 206802 (2005).
[39] K. Okumura, D. M. Jonas, and Y. Tanimura, Chem. Phys. **266**, 237 (2001).
[40] R. Haydock, V. Heine, and M. J. Kelly, J. Phys. C **5**, 2845 (1972).

[41] F. Guinea, C. Tejedor, F. Flores, and E. Louis, Phys. Rev. B **28**, 4397 (1983).
[42] E. N. Economou, *Green's Functions in Quantum Physics* (Springer-Verlag, Berlin, 1983).
[43] G. P. Srivastava, *The Physics of Phonons* (Adam Hilger, Bristol, 1990).
[44] J. E. Lennard-Jones, Proc. Phys. Soc. London **43**, 461 (1931).
[45] F. H. Stillinger and T. A. Weber, Phys. Rev. B **31**, 5262 (1985).
[46] D. D. Johnson, Phys. Rev. B **38**, 12807 (1988).
[47] N. W. Ashcroft and N. D. Mermin, *Solid State Physics*, (Harcourt, New York, 1976).